

SELF-CANCELLATION OF EPHEMERAL REGIONS IN THE QUIET SUN

SHUHONG YANG¹, JUN ZHANG¹, TING LI¹, YANG LIU²*Accepted for publication in ApJL*

ABSTRACT

With the observations from the Helioseismic and Magnetic Imager aboard the *Solar Dynamics Observatory*, we statistically investigate the ephemeral regions (ERs) in the quiet Sun. We find that there are two types of ERs: normal ERs (NERs) and self-cancelled ERs (SERs). Each NER emerges and grows with separation of its opposite polarity patches which will cancel or coalesce with other surrounding magnetic flux. Each SER also emerges and grows and its dipolar patches separate at first, but a part of magnetic flux of the SER will move together and cancel gradually, which is described with the term “self-cancellation” by us. We identify 2988 ERs among which there are 190 SERs, about 6.4% of the ERs. The mean value of self-cancellation fraction of SERs is 62.5%, and the total self-cancelled flux of SERs is 9.8% of the total ER flux. Our results also reveal that the higher the ER magnetic flux is, (i) the easier the performance of ER self-cancellation is, (ii) the smaller the self-cancellation fraction is, and (iii) the more the self-cancelled flux is. We think that the self-cancellation of SERs is caused by the submergence of magnetic loops connecting the dipolar patches, without magnetic energy release.

Subject headings: Sun: activity — Sun: photosphere — Sun: surface magnetism

1. INTRODUCTION

Ephemeral regions (ERs) are short-lived small-scale dipolar magnetic regions which were described by Harvey & Martin (1973) for the first time. According to the early results, ERs have a typical lifetime of 1–2 days and a dimension of 30 000 km with a maximum total flux of the order of 10^{20} Mx (Harvey & Martin 1973). In the following years, the lifetime of ERs determined with higher cadence observations was found to be much shorter, from around 12 hr (Harvey et al. 1975) to less than 3 hr (Title 2000), and the magnetic flux was found to be smaller ($\sim 10^{19}$ Mx; Schrijver et al. 1998; Chae et al. 2001).

In the quiet Sun, magnetic flux disappears due to cancellation and dispersion, but at the same time it is continuously replenished by newly emerged ERs. It takes only about one day for once replacement of the flux in the quiet photosphere (Schrijver et al. 1998; Hagenaar et al. 2003). Harvey et al. (1975) compared the parameters of ERs and regular active regions and argued that ERs are the small-scale end of a broad spectrum of magnetic activity. The results from Martin (1988) and Hagenaar et al. (2003) reveal that ERs likely vary in anti-phase with the solar cycle. The origin of ERs is still not well known. The source may be the recycled flux from decayed active regions (Nordlund 1992; Ploner et al. 2001). Alternatively, they may be produced through local dynamo processes, i.e., formed as a consequence of convective motions closer to the surface (Hagenaar et al. 2003; Stein et al. 2003). Hagenaar et al. (2008) studied the distribution and evolution of network magnetic elements in the quiet Sun and found that the emergence rate of ERs depends on the imbalance of magnetic flux

surrounding the emergence sites.

Yang et al. (2009) investigated magnetic field evolution in a coronal hole region. They reported that an ER emerged and its dipolar patches separated first and then moved together and cancelled with each other. With the help of vector magnetic fields and Doppler observations from the *Hinode*, they concluded that the cancellation between the opposite polarities of the ER was due to the submergence of original loops that emerged from below the photosphere. Recently, Wang et al. (2012) studied the solar intranetwork magnetic elements in a quiet region and an enhanced network area using the Narrow-band Filter Imager (NFI) magnetograms from the *Hinode*, and found an intranetwork dipolar flux emergence followed by cancellation of its two poles with opposite polarities. They believed that, after emergence, the dipolar flux indeed submerged, i.e., retracted back into the sub-photosphere again, because they had tracked the dipole continuously in the magnetograms with high temporal and spatial resolutions.

Then one question is raised: in the quiet Sun, how often and to what extent do ERs perform the behavior as reported by Yang et al. (2009) and Wang et al. (2012), i.e., an ER cancelling itself after emergence? The present paper is dedicated to answering this question based on statistical results.

2. OBSERVATIONS AND DATA ANALYSIS

The Helioseismic and Magnetic Imager (HMI; Scherrer et al. 2012; Schou et al. 2012) on board the *Solar Dynamics Observatory* (SDO; Pesnell et al. 2012) provides magnetic fields in the full-disk of the Sun with a pixel size of $0''.5$ and a cadence of 45 s uninterruptedly. In this paper, we adopt the HMI full-disk line-of-sight magnetograms with a 3 min cadence, i.e., one frame in four, from 2010 June 11 12:00 UT to 2010 June 15 12:00 UT.

For each point (x, y) on the solar disk, the heliocentric

¹ Key Laboratory of Solar Activity, National Astronomical Observatories, Chinese Academy of Sciences, Beijing 100012, China; [shuhongyang;jun;ting]@nao.cas.cn

² W.W. Hansen Experimental Physics Laboratory, Stanford University, Stanford, CA 94305-4085, USA; yliu@sun.stanford.edu

13-Jun-2010 11:59:03.500 UT

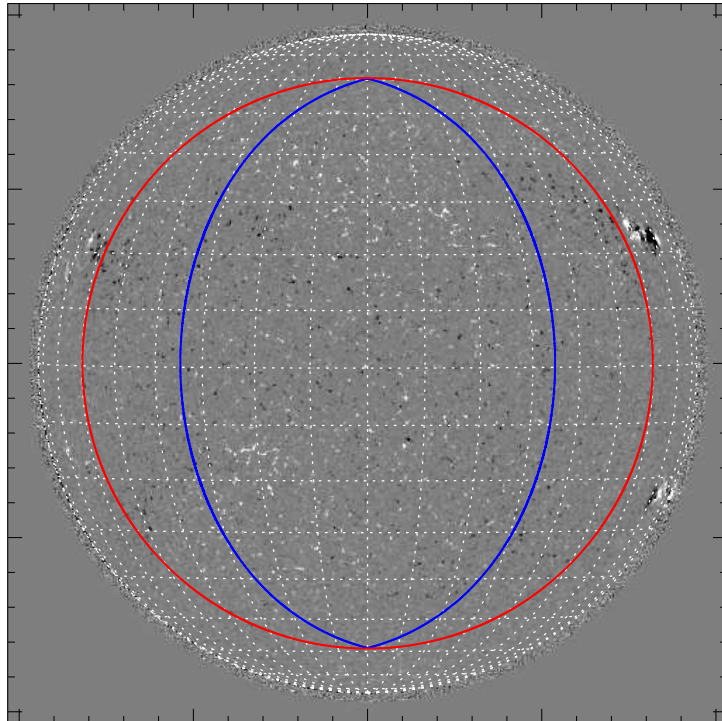


FIG. 1.— Line-of-sight magnetogram obtained by the *SDO*/HMI. The red circle delineates the area where the heliocentric angles are smaller than 60° . The blue curve outlines the pixels with heliocentric angles smaller than 60° at all the times from 2010 June 11 12:00 UT to 2010 June 15 12:00 UT considering the differential rotation of the Sun.

angle α is defined as: $\sin(\alpha) = \sqrt{x^2 + y^2}/R_\odot$, where R_\odot is the solar radius and the disk center is at $x = y = 0$. Since the noise increases for large α , we do not consider the pixels with $\alpha \geq 60^\circ$ in each magnetogram as Hagenaar (2001) and Jin et al. (2011) have done. In Figure 1, the red circle outlines the area where $\alpha < 60^\circ$. Then we derotate all the magnetograms differentially to a reference time (2010 June 13 12:00 UT). Our target area is outlined with the blue curve within which $\alpha < 60^\circ$ at all the times during the observation period of our data set.

For each pixel in the rotated frame, there is a certain α_0 . The pixel area S in the HMI magnetograms is $0''.5 \times 0''.5$, and one pixel at α_0 corresponds to a real area $S/\cos(\alpha_0)$ on the solar surface. The observed flux density B is assumed to be related to the flux density along the local normal direction, and then the corrected flux density is $B/\cos(\alpha_1)$, where α_1 , instead of α_0 , is the real position at the observation time.

3. RESULTS

We track the ERs that emerged within the area outlined by the blue curve in Figure 1, and identify 2988 ERs during the four days. We find that these ERs can be classified into two types according to their performance during evolution: normal ERs (NERs) and self-cancelled ERs (SERs). For each type, we provide one movie including three examples.

3.1. Type one: NERs

As can be seen from Movie 1 (available in the online edition), each NER emerged and grew with separation of its opposite polarity patches which cancelled or coalesced

with other magnetic flux at the end. Most of ERs are NERs, and the number of NERs is 2798.

The first example of NERs is shown in Figure 2. In the ellipse region, the NER emerged and could be identified as a dipolar region at 20:32 UT on June 13 (denoted by arrows in panel (a)). The two patches with opposite polarities (labeled with “A” and “B”) grew and separated along the long axis (panel (b)). The negative patch moved toward the pre-existing positive magnetic field (indicated by arrow “C”) and cancelled with each other (panel (c)). At 02:05 UT on June 14, most flux of “A” had disappeared and the cancellation between “A” and “C” was still going on (panel (d)).

Along slit “M—N” marked in panel (c), we obtain the image profile by averaging five pixels in the magnetograms in the direction perpendicular to “M—N”. Then we make the space-time plot of such profiles over time from June 13 17:29 UT to June 14 04:56 UT, as displayed in panel (e). The NER emerged around 18:30 UT and the two patches separated with an average velocity of 0.8 km s^{-1} in the first three hours (marked by the dashed lines). Moreover, during the emerging stage, there was a rapid emergence with an expansion velocity of 3.9 km s^{-1} from 20:29 UT (marked by the dotted lines). After 21:30 UT, when the NER was well developed, the separation slowed down, and patch “A” moved toward “C” and cancelled with it.

We measure the magnetic flux (ϕ) of the NER by calculating ϕ_+ and ϕ_- in an area containing the two patches. The selected area is changed according to the expansion of the NER to ensure that the area has an appropriate size. After selection, the pixels with unsigned magnetic fields weaker than 10.2 Mx cm^{-2} (noise level determined

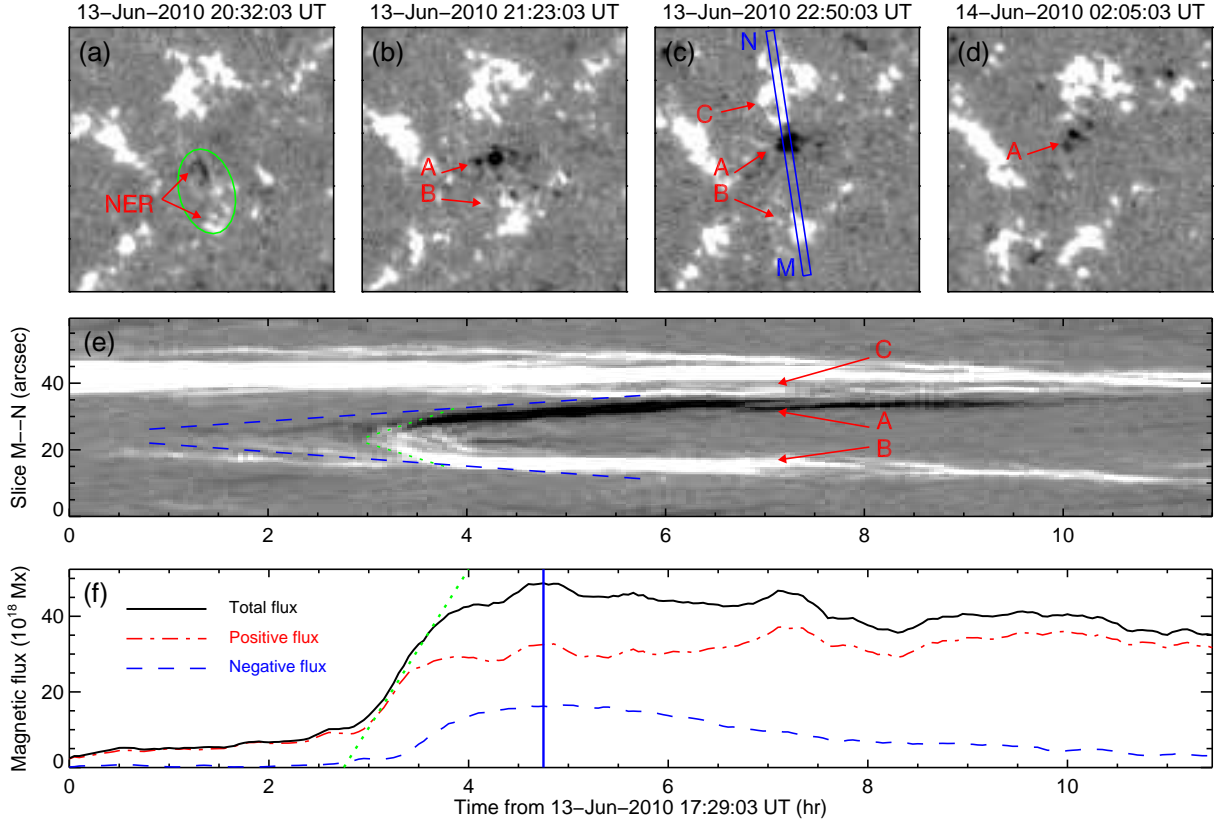


FIG. 2.— Panels (a)–(d): sequence of HMI magnetograms displaying the evolution of a NER denoted by the arrows and outlined by the ellipse in panel (a). The field-of-view is $50'' \times 50''$ and the grayscale saturates at ± 80 Mx cm^{-2} . Arrows “A”, “B”, and “C” denote the negative and the positive patches of the NER and the pre-existing positive magnetic fields, respectively. Panel (e): space-time plot along slit “M–N” marked in panel (c). The dashed lines indicate the separation of the NER patches, and the dotted lines a rapid emergence phase of the NER. Panel (f): temporal variations of the positive (dash-dotted curve), negative (dashed curve), and total (solid curve) magnetic flux of the NER. The dotted line indicates a sharp increase of total magnetic flux and the solid vertical line marks the flux maximum.

by Liu et al. 2012) are eliminated. The positive flux ($|\phi_+|$), negative flux ($|\phi_-|$), and total flux ($|\phi_+| + |\phi_-|$) are plotted as a function of time in panel (f). The total flux displayed a sharp increase at a rate of 4.2×10^{19} Mx hr^{-1} during the rapid emergence stage (20:29 UT — 21:11 UT) and then appeared as a slow increase and reached 4.8×10^{19} Mx. From 22:20 UT when the negative patch “A” collided and cancelled with the pre-existing positive patch “C”, the negative flux of the NER began to decrease at a rate of 2.2×10^{18} Mx hr^{-1} , while the positive flux of the NER mainly maintained at a steady level.

3.2. Type two: SERs

As shown in Movie 2 (available in the online edition), each SER emerged and grew and its dipolar patches separated at first, but then a part of magnetic flux of the SER moved together and cancelled gradually, which is described with the term “self-cancellation” by us in this paper. There are only 190 SERs, about 6.4% of the ERs.

Figure 3 shows the evolution of the first SER in Movie 2. The ellipse region in panel (a) outlines the location of the SER. At 08:11 UT on June 14, the SER (indicated by arrows in panel (a)) had exhibited a significant dipolar configuration. Then the SER went on developing and its two patches (denoted by arrows “A” and “B” in panel (b)) separated. Gradually, the positive polarity patch “A” split into two major elements “A1” and “A2”, and

“A2” moved toward to “B” while “A1” and “B” did not change their positions a lot (panel (c)). When “A2” met with “B”, the cancellation took place (see panel (d)), and at last, “A2” completely disappeared and part of “B” was remained.

Along the separation and approach direction, i.e., “M–N” marked in panel (d), we obtain a series of image profiles as we have done in Figure 2, and stack them in panel (e). The changes of positive flux, negative flux, and total flux ($|\phi_+|$, $|\phi_-|$, and $|\phi_+| + |\phi_-|$, respectively) during this period are shown in panel (f). The SER violently emerged with the negative patch followed by the positive one (the first three hours in panel (e)), leading to a rapid increase of total flux to 1.1×10^{20} Mx and an imbalance between the positive and the negative flux at the emergence stage (stage 1 in panel (f)). When the SER was well developed, expansion of the two patches (positive “A” and negative “B” in panel (e)) almost stopped, and patch “A” began to split into two components, “A1” and “A2”. Component “A2” moved toward to “B” (marked by the red dotted line in panel (e)) and met with “B” around 22:15 UT (marked by the dotted vertical line in panel (f)). Then, “A2” began to cancel with “B”, resulting in the total disappearance of “A2” and the shrinkage of “B”. This self-cancellation process led to the significant decrease of total magnetic flux from 6.4×10^{19} Mx to 4.4×10^{19} Mx at a rate of 1.3×10^{19} Mx hr^{-1} (marked by the red dotted line in panel (f)).

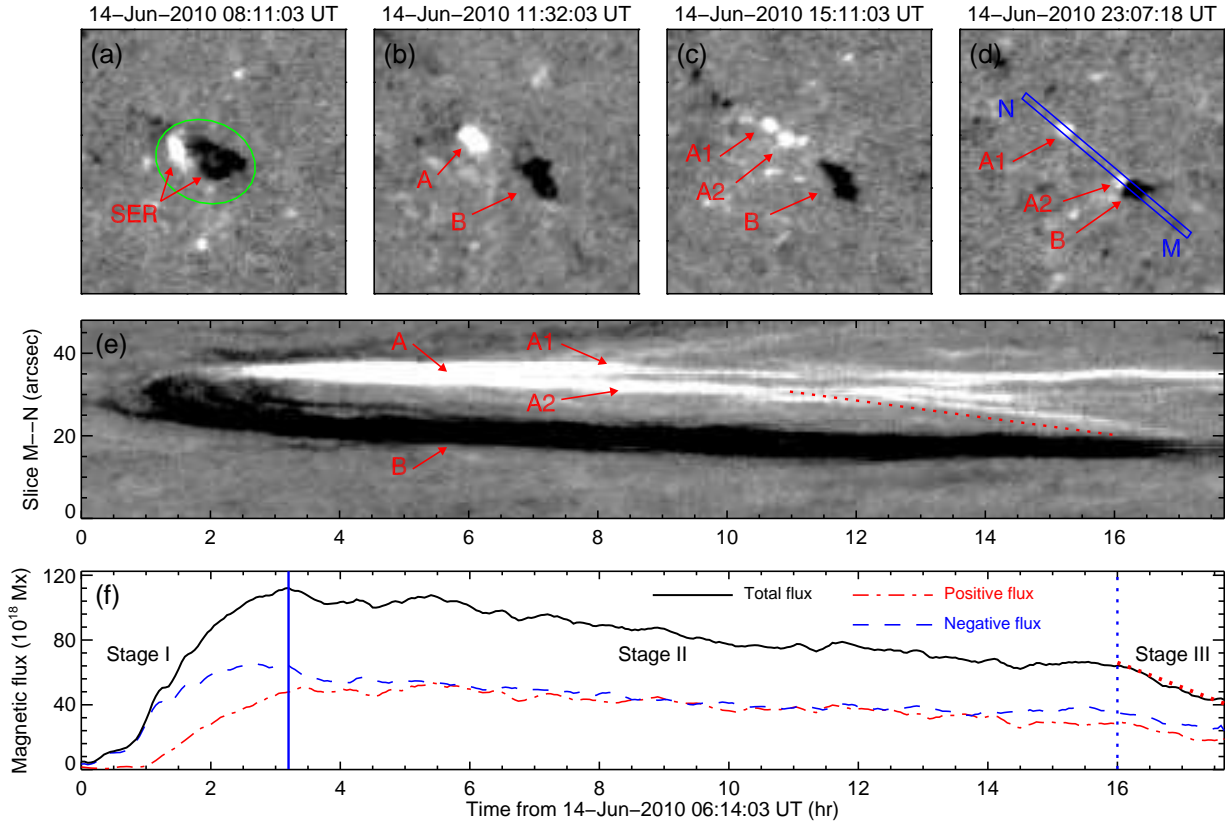


FIG. 3.— Similar to Figure 2 but for the evolution of a SER. Magnetic elements “A1” and “A2” are two components splitting from the positive patch of the SER. The dotted line in panel (e) marks the movement of element “A2”. The red dotted line in panel (f) indicates the decrease of total magnetic flux due to the cancellation between “A2” and “B”, and the dotted vertical line marks the start time of the cancellation.

3.3. Statistical results of the ERs

The probability density functions (PDFs) of the ER (black curve) and SER (red curve) numbers are plotted in Figure 4(a). We find that the PDF peak of the ERs is at 5.0×10^{18} Mx, and there is also a peak of the SER PDF which can be seen clearly in panel (b). The PDF of SERs is peaked at 1.8×10^{19} Mx. The blue curve in panel (a) represents the number ratio of SER to ER. The dash-dotted vertical line is located at 5.5×10^{19} Mx, a general separation of abundant samples (before) and few samples (after). Thus, we think the ratio curve before the vertical line is statistically reliable. The ratio curve increases from 0 to 0.5 with the variation of ER flux from 0 to 5.5×10^{19} Mx, revealing that the higher the ER magnetic flux is, the easier the performance of ER self-cancellation is.

For SERs, only part of magnetic flux is self-cancelled. The scatter plots of self-cancellation fractions versus magnetic flux of SERs are shown with red symbols in Figure 4(c). The mean value of self-cancellation fraction of SERs is 62.5%. We apply a “sort-group” method introduced by Zhao et al. (2009) to the SERs: (1) all the SERs are sorted according to the total magnetic flux of individuals; (2) the 190 sorted SERs are grouped into 10 data points with equal SER number and each data point is assigned with the mean value of the corresponding SER group; (3) the self-cancellation fractions and the magnetic flux values are correlated with each other and plotted with blue symbols in Figure 4(c). The statistical correlation shows a general tendency that the higher

the ER magnetic flux is, the smaller the self-cancellation fraction is. We plot the PDF of self-cancellation fractions in panel (d). The dotted vertical line marks the PDF maximum at 75%. We can see that there are an increase and a decrease trends before and after the PDF peak, respectively.

Figures 4(e) and 4(f) are similar to Figures 4(a) and 4(b), but for ER flux (black curve), self-cancelled flux (red curve), and the ratio (blue curve) of self-cancelled flux to ER flux. The PDF of ER flux is peaked at 7.0×10^{18} Mx (panel (e)), and the peak of self-cancelled flux is at 3.3×10^{19} Mx (panel (f)). The flux ratio curve exhibits a variation from 0 to 0.3 in the range of 0 — 5.5×10^{19} Mx, indicating that the higher the ER magnetic flux is, the more the self-cancelled flux is.

4. CONCLUSIONS AND DISCUSSION

With the observations from the *SDO*/HMI, we statistically investigate the ERs in the quiet Sun. We find that there are two types of ERs: NERs and SERs. Each NER emerged and grew with separation of its opposite polarity patches which finally cancelled or coalesced with other magnetic flux. Each SER also emerged and grew and its dipolar patches separated at first, but then a part of magnetic flux of the SER moved together and cancelled gradually, which is described with the term “self-cancellation”. We identify 2988 ERs among which there are 190 SERs, about 6.4% of the ERs. The mean value of self-cancellation fraction of SERs is 62.5%, and the total self-cancelled flux of SERs is 9.8% of the total ER flux. Our results also reveal that the higher the ER

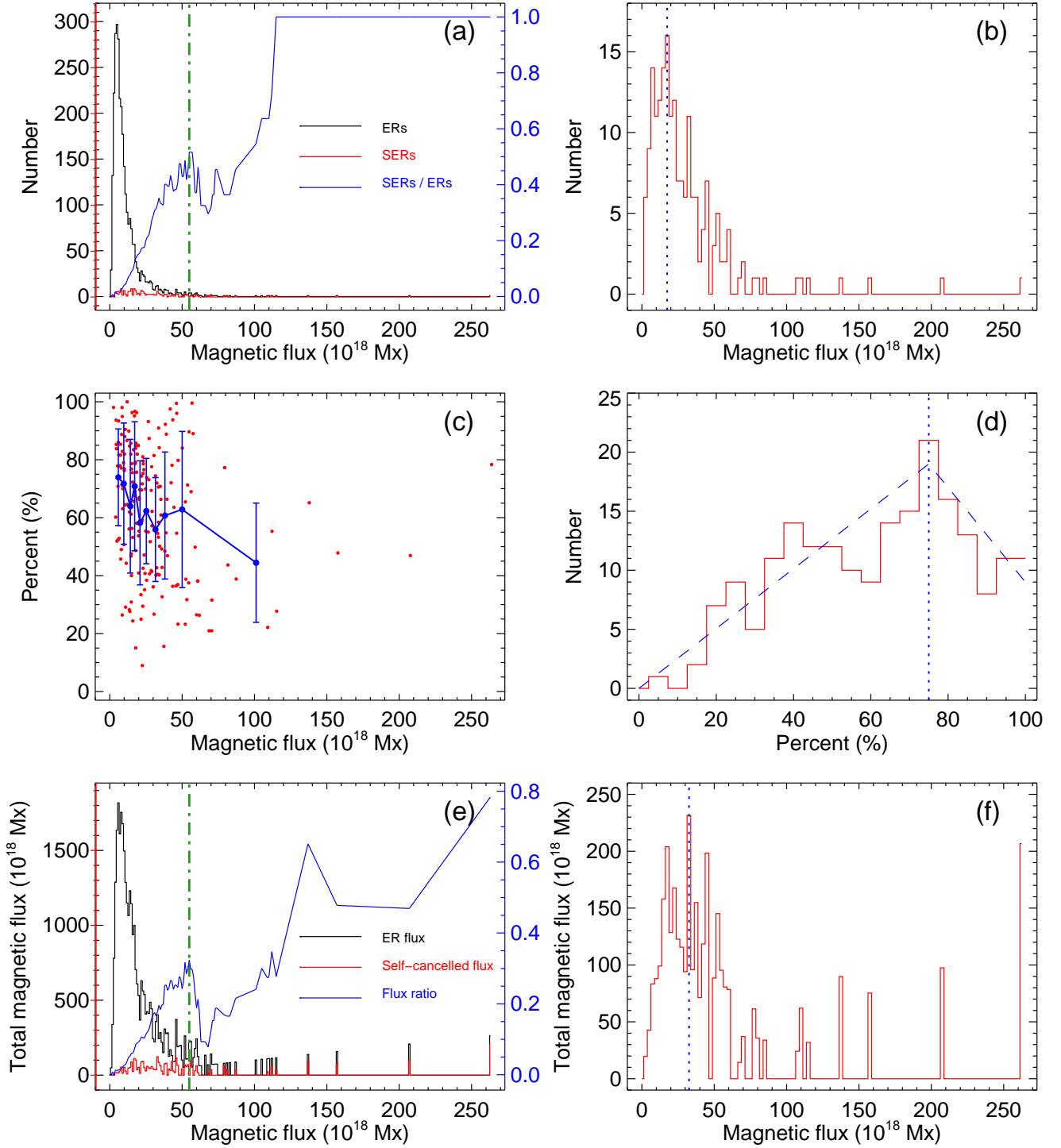


FIG. 4.— *Panel (a):* PDFs of ER (black curve) and SER (red curve) numbers and the number ratio (blue curve) of SER to ER. The binsize is 1×10^{18} Mx. The dash-dotted vertical line is located at 5.5×10^{19} Mx, a general separation of abundant samples (before) and few samples (after). *Panel (b):* PDF of SERs at an enlarged displaying scale with a binsize of 2×10^{18} Mx. The dotted vertical line marks the PDF maximum. *Panel (c):* scatter plots of self-cancellation fractions versus magnetic flux of SERs (red symbols) and of sorted and grouped points with error bars (blue symbols). *Panel (d):* PDF of self-cancellation fractions with a binsize of 5%. The dotted vertical line marks the PDF maximum before and after which there are increase and decrease trends (dashed lines). *Panels (e) and (f):* similar to panels (a) and (b), but for ER flux (black curve), self-cancelled flux (red curve), and the ratio (blue curve) of self-cancelled flux to ER flux.

magnetic flux is, (i) the easier the performance of ER self-cancellation is, (ii) the smaller the self-cancellation fraction is, and (iii) the more the self-cancelled flux is.

Magnetic flux cancellation is an observational phenomenon of flux disappearance when two magnetic patches with different polarities encounter (Livi et al. 1985; Martin et al. 1985; Zhang et al. 2001). As one of the three modes for removal of magnetic flux with opposite polarities from the photosphere illustrated by Zwaan (1978, 1987), the disappearance of magnetic flux can be resulted from the retraction of magnetic loops into the sub-photosphere, if the two poles are still connected by initial loops. So in theory, the process that magnetic loops emerge into the solar atmosphere and then submerge below the subsurface is quite reasonable and possible. The submergence of part of an active region was studied by Rabin et al. (1984) and the submergence of a sunspot group was reported by Zirin (1985) who suggested that submergence of an active region may be common. To determine if cancellation is caused by the submergence of magnetic loops, it is important to check vector field data. With *Hinode* spectro-polarimetric data, Yang et al. (2009) found that at the area where the two opposite polarities of the ER cancelled, there were strong transverse fields pointing directly from the positive patch to the negative one. Moreover, they also observed larger Doppler redshifts between the cancelling patches. They suggested that the cancellation of the ER was due to the submergence of original loops. In the recent study of Wang et al. (2012), although there was a lack of vector field observations, they believed that the emergence and submergence of the ER they observed was a real behavior since the ER had been tracked in the high temporal resolution photospheric magnetogram. Thus, we also think the self-cancellation of SERs is caused by the submergence of magnetic loops connecting the dipolar patches.

When magnetic patches of ERs separate and cancel with other magnetic elements, the connection between opposite polarities will be changed and the magnetic loops will be restructured to a lower potential configuration, which requires magnetic flux reconnection accompanied with energy release (Wang & Shi 1993). While when the ER loops emerge through the photosphere layer from below and then submerge into the sub-photosphere again, no magnetic reconnection occurs and no magnetic energy is released.

Our results reveal a tendency that the higher the ER magnetic flux is, the easier the performance of ER self-cancellation is. We suggest that the behaviour depends on the magnitude of magnetic flux and on the relative importance and balance between the magnetic pressure and the magnetic tension acting on the emerging flux tubes. In this study, we also notice that the dipolar patches of most of the SERs split before the self-cancellation phase (eg., as shown in Figure 3). It may be caused by plasma motions in the photosphere. When they emerge into the photosphere, they are drifted toward the supergranular boundaries by mesogranular and supergranular flow and split into smaller fragments due to granular convection (Simon et al. 2001; Priest et al. 2002).

We are grateful to the referee for helpful comments. We thank Prof. Jingxiu Wang for his valuable suggestions. This work is supported by the National Natural Science Foundations of China (40890161, 11025315, 10921303, 41074123 and 11003024), the CAS Project KJCX2-EW-T07, the National Basic Research Program of China under grant 2011CB811403, and the Young Researcher Grant of National Astronomical Observatories, Chinese Academy of Sciences. The data have been used by courtesy of NASA/*SDO* and the HMI science team.

REFERENCES

- Chae, J., Martin, S. F., Yun, H. S., et al. 2001, *ApJ*, 548, 497
Hagenaar, H. J. 2001, *ApJ*, 555, 448
Hagenaar, H. J., De Rosa, M. L., & Schrijver, C. J. 2008, *ApJ*, 678, 541
Hagenaar, H. J., Schrijver, C. J., & Title, A. M. 2003, *ApJ*, 584, 1107
Harvey, K. L., Harvey, J. W., & Martin, S. F. 1975, *Sol. Phys.*, 40, 87
Harvey, K. L., & Martin, S. F. 1973, *Sol. Phys.*, 32, 389
Jin, C. L., Wang, J. X., Song, Q., & Zhao, H. 2011, *ApJ*, 731, 37
Liu, Y., Hoeksema, J. T., Scherrer, P. H., et al. 2012, *Sol. Phys.*, in press.
Livi, S. H. B., Wang, J., & Martin, S. F. 1985, *Australian Journal of Physics*, 38, 855
Martin, S. F. 1988, *Sol. Phys.*, 117, 243
Martin, S. F., Livi, S. H. B., & Wang, J. 1985, *Australian Journal of Physics*, 38, 929
Nordlund, A., Brandenburg, A., Jennings, R. L., et al. 1992, *ApJ*, 392, 647
Pessnell, W. D., Thompson, B. J., & Chamberlin, P. C. 2012, *Sol. Phys.*, 275, 3
Ploner, S. R. O., Schüssler, M., Solanki, S. K., & Gadun, A. S. 2001, *Advanced Solar Polarimetry – Theory, Observation, and Instrumentation*, 236, 363
Priest, E. R., Heyvaerts, J. F., & Title, A. M. 2002, *ApJ*, 576, 533
Rabin, D., Moore, R., & Hagyard, M. J. 1984, *ApJ*, 287, 404
Schou, J., Scherrer, P. H., Bush, R. I., et al. 2012, *Sol. Phys.*, 275, 229
Scherrer, P. H., Schou, J., Bush, R. I., et al. 2012, *Sol. Phys.*, 275, 207
Schrijver, C. J., Title, A. M., Harvey, K. L., et al. 1998, *Nature*, 394, 152
Simon, G. W., Title, A. M., & Weiss, N. O. 2001, *ApJ*, 561, 427
Stein, R. F., Bercik, D., & Nordlund, Å. 2003, *Current Theoretical Models and Future High Resolution Solar Observations: Preparing for ATST*, 286, 121
Title, A. 2000, *Royal Society of London Transactions Series A*, 358, 657
Wang, J. X., & Shi, Z. X. 1993, *Sol. Phys.*, 143, 119
Wang, J. X., Zhou, G. P., Jin, C. L., & Li, H. 2012, *Sol. Phys.*, 278, 299.
Yang, S. H., Zhang, J., & Borrero, J. M. 2009, *ApJ*, 703, 1012
Zhang, J., Wang, J. X., Deng, Y. Y., & Wu, D. J. 2001, *ApJ*, 548, L99
Zhao, M., Wang, J. X., Jin, C. L., & Zhou, G. P. 2009, *RAA*, 9, 933
Zirin, H. 1985, *ApJ*, 291, 858
Zwaan, C. 1978, *Sol. Phys.*, 60, 213
Zwaan, C. 1987, *ARA&A*, 25, 83